Simulation of Steady, Laminar Flow Over a Backward-Facing Step

Sagar Bhatt
Masters Student
Department of Mechanical and Aerospace Engineering,
University at Buffalo

Contents

List of Figures

Abstract

A 2D Navier-Stokes solver was developed to simulate steady,laminar flow over a backward-facing step of height h. The step expansion ratio=1/2 and the flow at the step was assumed to be fully developed, laminar channel flow. The Reynolds number for this flow was defined as Re=Uh/ν. The 2D incompressible Navier-Stokes equations was solved in generalized curvilinear coordinates using artificial compressibility method. A code was developed using MATLAB where three-point , second order finite differencing was used to discretize the convective and viscous fluxes in conjunction with scalar, fourth-difference, third-order artificial dissipation for stability. Dual time-stepping with a second-order backward scheme in real time and four stage Runge-Kutta time stepping was used for pseudo time. The flow was simulated for Re_h=50, 100, 200, and 400. The streamlines were plotted in the steady-state. The results were compared with the experimental data obtained by Armaly et al.[2] and the numerical solutions obtained by Kim and Moin[11]. The effects of local time stepping, implicit residual smoothing and the CFL number are investigated on the rate of convergence of the time algorithm. The effect of artificial dissipation on the accuracy and stability of the solution is also investigated. The results are in agreement with the experimental and numerical solutions of Armaly et al. and Kim and Moin.

I. Introduction

This project is concerned with simulating a 2D laminar flow over a backward-facing step. Although numerous investigations have been carried out on this subject, the exact physical origins of the flow separation and vortex formation has not been clear owing to the fact that the analytical treatment of the flow is not available and hence experimental and numerical investigations are involved [3]. Fluid flow problems in channels with separation and reattachment of boundary layer is encountered in many real world situations such as ducts, heat exchangers etc[8]. Hence, study of such phenomenon is vitally important. When studying such flow problems, backward-facing step can be regarded has having one of the simplest geometries while retaining rich flow physics manifested by flow separation, flow reattachment and multiple recirculating bubbles in the channel depending on the Reynolds number and the geometrical parameters such as the step height and the channel height[8].

The study of backward-facing step flows is an important part of fundamental fluid mechanics. Among the numerous studies that have been undertaken on the subject, the works of Armaly *et al.* stands apart. They presented a detailed experimental and numerical investigation in a backwards-facing geometry for an expansion ratio of H/h=2, an aspect ratio W/h=36 and Reynolds numbers up to Re_D=8000. They reported multiple recirculation zones downstream of the step. Kim and Moin[11] computed flow over a backward-facing step using Fractional Step method, which is second order accurate in both space and time. They investigated the dependence of reattachment length on Reynolds number.Their results were in good agreement with Armaly *et al.* to about Re_D =500. For Re_D >500, their results started to deviate from the experimental data. This was attributed to the three dimensional nature of the flow. The three dimensionality of the flow was investigated by Biswas *et al.* for $Re_D \leq$800.Their results were in agreement with experimental results of Armaly *et al.*. The definition of Reynolds number used by Armaly *et al.* is given by $Re_D = \frac{UD}{\nu}$, where U is two-thirds of maximum inlet velocity, D is the hydraulic diameter of the inlet channel which is twice its height, *i.e.* D=2h, and ν is the kinematic viscocity. In our study, Re has been defined as $Re_h = \frac{Uh}{\nu}$. Hence, the cases we are considering, Re_h=50, 100, 200 and 400 correspond to Re_D=100, 200, 400 and 800, respectively, from Armaly *et al.*'s work. This relation will help us in comparing our results to that of Armal *et al.* and Kim and Moin's results.

I. Backward Facing Step Flow

As reported numerous times in literature, backward-facing step flows result in formation of two major recirculation zones. The primary recirculation zone occurs right after the step in the lower region between the step and the floor of the cavity. The secondary recirculation zone occurs on the upper wall of the cavity after the primary recirculation zone has ended. One of the targets of this study is to investigate formation of these zones and their dependence on the Reynolds number.

The setup of the problem is shown in figure 1. The expansion ratio of h:H=1:2. The aspect ratio of the setup, h:L=1:20 where, L=length of the channel.

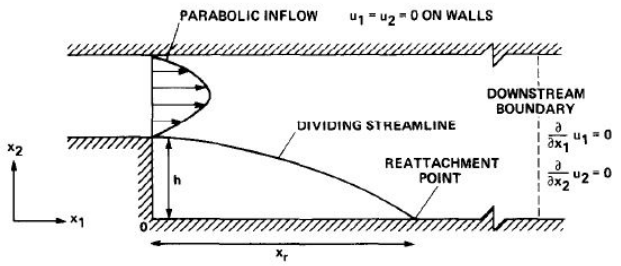

Figure 1: *Setup of the problem*

II. Governing Equations

An incompressible fluid with constant properties is assumed. Non-dimensionalized Navier-Stokes equations in Cartesian co-ordinates are given by:

$$\Gamma\frac{\partial Q}{\partial t} + \frac{\partial E^1}{\partial x} + \frac{\partial E^2}{\partial y} - \frac{\partial E_v^1}{\partial x} - \frac{\partial E_v^2}{\partial y} = 0$$

where,

$$\Gamma = diag(0, 1, 1) \ ,$$

$$Q = \begin{bmatrix} P \\ u \\ v \end{bmatrix} \ , \ E^1 = \begin{bmatrix} u \\ uu + P \\ uv \end{bmatrix} \ ,$$

$$E^2 = \begin{bmatrix} v \\ uv \\ vv + P \end{bmatrix} \ , \ E_v^1 = \frac{1}{Re}\begin{bmatrix} 0 \\ \partial u \ \partial x \\ \partial v \ \partial x \end{bmatrix} \ ,$$

$$E_v^2 = \frac{1}{Re}\begin{bmatrix} 0 \\ \partial u \ \partial y \\ \partial v \ \partial y \end{bmatrix}$$

The numerical solution of these equations presents major difficulties, due in part to the special role of the pressure in the equations and in part to the large amount of computer time which such solution usually requires, making it necessary to devise finite-difference schemes which allow efficient computation. In two-dimensional problems the pressure can be eliminated from the equations using the stream function and vorticity, thus avoiding one of the difficulties[6]. Chorin developed a method called "Method of Artificial Compressibilty"[6] and since then has been improved by numerous researchers for solving unsteady Navier-Stokes equations. This method is,typically, combined with dual time stepping where an iteration in dual time is implemented for each time step in real time. This method assures a convergence of solution for incompressible unsteady problem[12]. Chorin himself implemented the method using DuFort-Frankel scheme on a standard grid in the 2D case of thermal convection in a fluid layer heated from below [6]

II. Method of Solution

Firstly, the generalized coordinate transformation was achieved for curvilinear coordinate system $(x, y) \rightarrow (\xi, \eta)$ where $\xi = \xi(x, y), \eta = \eta(x, y)$. For this purpose first x_ξ, x_η, y_ξ and y_η were calculated. This was achieved by using forward differencing of x and y and taking $\Delta\xi, \Delta\eta = 1$. For example:

$$\frac{\partial x}{\partial \xi} = \frac{x_{i+1} - x_{i-1}}{\Delta\xi}$$

Using these values Jacobian was calculated in the following manner:

$$G = det\begin{bmatrix} x_\xi & y_\xi \\ x_\eta & y_\eta \end{bmatrix} = x_\xi y_\eta - x_\eta y_\xi$$

Jacobian: $J = \dfrac{1}{G}$

Then metrics of transformation were calculated using the following:
$\xi_x = Jy_\eta, \ \xi_y = -Jx_\eta, \ \eta_x = -Jy_\xi, \ \eta_y = Jx_\xi$

Using these, metric tensor was calculated:

$$g^{ij} = \begin{bmatrix} g^{11} & g^{12} \\ g^{12} & g^{22} \end{bmatrix} = \begin{bmatrix} (\xi_x)^2 + (\xi_y)^2 & \xi_x\eta_x + \xi_y\eta_y \\ \xi_x\eta_x + \xi_y\eta_y & \xi_x)^2 + (\xi_y)^2 \end{bmatrix}$$

Now, covariant velocities were calculated using:
$U = u\xi_x + v\xi_y, \ V = u\eta_x + v\eta_y$

Hence now we can do a partial transformation of non-dimensionalised Navier-Stokes equation in curvilinear co-ordinates:

$$\frac{1}{J}\Gamma\frac{\partial Q}{\partial t} + \frac{\partial E^{*1}}{\partial \xi} + \frac{\partial E^{*2}}{\partial \eta} - \frac{\partial E_v^{*1}}{\partial \xi} - \frac{\partial E_v^{*2}}{\partial \eta} = 0$$

where,

$$\Gamma = diag(0, 1, 1) \ ,$$

$$E^{*1} = \frac{1}{J}\begin{bmatrix} U \\ uU + P\xi_x \\ vU + P\xi_y \end{bmatrix},$$

$$E^{*2} = \frac{1}{J}\begin{bmatrix} V \\ uV + P\eta_x \\ vV + P\eta_y \end{bmatrix},$$

$$E_v^{*1} = \frac{1}{Re}\frac{1}{J}\begin{bmatrix} 0 \\ g^{11}\dfrac{\partial u}{\partial \xi} + g^{12}\dfrac{\partial u}{\partial \eta} \\ g^{11}\dfrac{\partial v}{\partial \xi} + g^{12}\dfrac{\partial v}{\partial \eta} \end{bmatrix},$$

$$E_v^{*2} = \frac{1}{Re}\frac{1}{J}\begin{bmatrix} 0 \\ g^{12}\dfrac{\partial u}{\partial \xi} + g^{22}\dfrac{\partial u}{\partial \eta} \\ g^{12}\dfrac{\partial v}{\partial \xi} + g^{22}\dfrac{\partial v}{\partial \eta} \end{bmatrix}$$

The viscous and convective fluxes were then discretized using three-point, second order accurate finite differencing. Central differencing satisfies these requirements. The finite difference equations for this method is given by:

$$\frac{\partial u}{\partial x} = \frac{u_{i+1} - u_{i-1}}{2\Delta x}$$

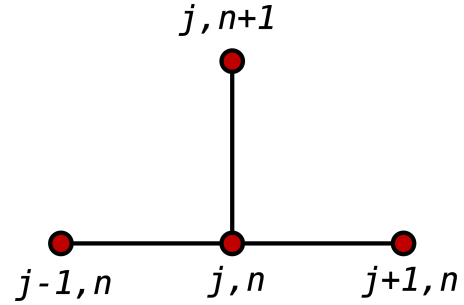

Figure 2: *Stencil of three point central differencing*

Using this discretization, the convective and viscous fluxes were calculated and then right hand side of the Navier-Stokes equations were calculated. One of the major challenges in computing solutions to the incompressible Navier-Stokes system of PDEs s satisfying the divergence-free velocity condition. For this purpose, Artificial Compresssibility method was used. Artificial compressibility method [6], provides a mechanism to march in pseudo-time for each real time step to achieve divergence-free velocity field such that mass and momentum are conserved in the steady-state. The classical artificial compressibility method transforms the mixed elliptic/parabolic type equations into a system of hyperbolic or parabolic equations in pseudo-time, which can be numerically integrated. The method has been generalized to curvilinear coordinates.The compressible Navier-Stokes equations are hyperbolic in nature i.e. they have real characteristics whereas the incompressible flow equations are mixed parabolic-elliptic in nature. Using method the hyperbolic nature of the compressible Navier-Stikes equations is given to the incom- pressible equation by adding the time derivative of the pressure in continuity equations.The odd derivatives in the truncation error causes dispersive effects which result in numerical oscillations in the solution. For this purpose artificial dissipation was introduced in the system to reduce ossilations in the calculated RHS.

To calculate artificial dissipation, first the Jacobian matrix is calculated as follows:

$$A^j = \frac{1}{J}\begin{bmatrix} 0 & \xi_x^j & \xi_y^j \\ \xi_x^j & U^j + u\xi_x^j & u\xi_y^j \\ \xi_y^j & v\xi_x^j & U^j + v\xi_y^j \end{bmatrix},$$

$\xi^1 = \xi,\ \xi^2 = \eta\ , and$

$U^1 = U\ , U^2 = V$

Now, the spectral radius was calculated using:

$$\rho(A^j) = \frac{1}{J}(|U^j| + \sqrt{(U^j)^2 + g^{jj}})$$

Now, the dissipation was calculated using the following finite difference equations:

$$Diss_{(i,j)} = \widetilde{\delta_\xi} D^1_{(i,j)} + \widetilde{\delta_\eta} D^2_{(i,j)} = (D^1_{(i+1/2,j)} - D^1_{(i-1/2,j)}) + (D^2_{(i,j+1/2)} - D^2_{(i,j-1/2)})$$

$$D^1_{(i+1/2,j)} = \epsilon\rho(A^1)(Q_{(i+2,j)} - 3Q_{(i+1,j)} + 3Q_{(i,j)} - Q_{(i-1,j)})$$

Where ϵ is a small number which controls the dissipation. RHS with artificial dissipation was then used in time marching inorder to calculate pressure, x-velocity and y-velocity of the the flow field. For time marching, dual time stepping technique was used. The Artificial compressibility equaltions wih dual time-stepping are given by:

$$\frac{\partial Q}{\partial \tau} = -\Gamma \frac{\partial Q}{\partial t} - J\left(\frac{\partial E^{*1}}{\partial \xi} + \frac{\partial E^{*2}}{\partial \eta} - \frac{\partial E_v^{*1}}{\partial \xi} - \frac{\partial E_v^{*2}}{\partial \eta} + Diss\right) = RHS$$

Discretization of real time component of dual time stepping was discretized using second order backward differencing. The finite difference equation for this scheme is given by:

$$\frac{\partial Q}{\partial t} = \frac{3Q^{n+1} - 4Q^n + Q^{n-1}}{2\Delta t}$$

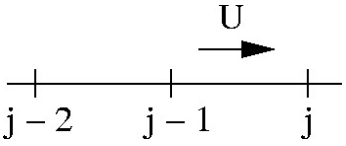

Figure 3: *Stencil of second order backward differencing*

Pseudo time marching was achieved by implementing fourth stage Runge-Kutta scheme, the finite difference equation for which is given by:

$$Q^{k+1,1} = Q^k + \frac{1}{4}\Delta\tau RHS$$

$$Q^{k+1,2} = Q^k + \frac{1}{3}\Delta\tau RHS^1$$

$$Q^{k+1,3} = Q^k + \frac{1}{2}\Delta\tau RHS^2$$

$$Q^{k+1} = Q^k + \Delta\tau RHS^3$$

where, $\Delta\tau$ is the local time step for the pseudo time marching. This time step is not a constant value but varies for each grid point. The pseudo time stepping is more efficient if the time step varies for each grid point depending the CFL and Von-Neumann number. The pseudo time step is given by:

$$\Delta\tau_{i,j} = min\left(\frac{CFL}{J \times max(\rho(A^1), \rho(A^2)}, \frac{Re * VN}{max(g^{11}, g^{22})}\right)$$

For each real time step, the solution was marched in pseudo time until it reached solution. The program was executed for different grid sizes, stretching ratios and time steps to verify accuracy of the code. The results are discussed later.

The pseudo time marching does not march the solution itself in time but helps in reducing the residual and to get a divergence free velocity condition. We can increase convergence rate of this method by reducing the residuals before marching in pseudo time. One of the methods to achieve this is the implicit residual smoothing. This technique helps in reducing the fluctuations of the residuals and to increase the size of time step hence increasing the speed of time marching. The equation to achieve residual smoothing is given by:

$$(1 - \varepsilon_\xi \delta_{\xi\xi})(1 - \varepsilon_\eta \delta_{\eta\eta})\overrightarrow{\overline{RHS}} = \overrightarrow{RHS}$$

where, $\overrightarrow{RHS}$is the computed RHS and $\overrightarrow{\overline{RHS}}$ is the smoothed RHS. Direct dicretization of this equation results in a pentadiagonal matrix which is tedious and computationally expensive (O(N^3)). This pentadiagonal matrix is broken into two tridiagonal systems by the following equations:

$$(1 - \varepsilon_\xi \delta_{\xi\xi})\overrightarrow{U_{i,j}} = \overrightarrow{RHS}$$

$$U_{i,j} - \varepsilon \frac{U_{i+1,j} - 2Ui, j + Ui - 1, j}{\Delta\xi^2} = \overrightarrow{RHS_{i,j}}$$

$$\overline{RHS}_{i,j} - \varepsilon \frac{\overline{RHS}_{i,j+1} - 2\overline{RHS}_{i,j} + \overline{RHS}_{i,j-1}}{\Delta\eta^2} = U_{i,j}$$

The resulting tridiagonal system will be much faster and cheaper (O(N)).

Boundary Conditions: The boundary condition for the problem are:

Walls: U=V=0; $\frac{\partial P}{\partial n} = 0$

Inlet: U=1 (Normalized, Parabolic profile) , V=0;

Exit: $\frac{\partial U}{\partial x} = 0, \frac{\partial V}{\partial x} = 0$

III. Grid generation

Since the problem is a 2D cavity flow, the domain is a rectangle where aspect ratio=1:20.For this domain both uniform and stretched grids were generated. For uniform grid, a constant spacing of Δx was chosen. Figure 4 shows a uniform grid for the given domain. The solution was calculated for successively finer grids for a uniform grid until grid independence was achieved. For representation purpose, smaller grid of dimensions 61X61 is shown here.

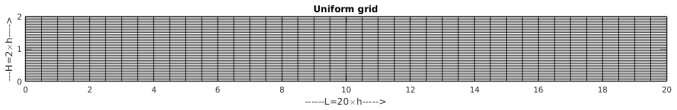

Figure 4: *A 61X61 uniform grid*

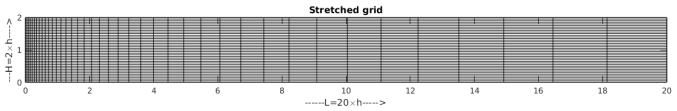

Figure 5: *A 61X61 stretched grid with stretching ratio=1.1*

For stretched grids, grid was made finer in the first half of the domain where the recirculation was expected and then it was allowed to get coarse since the flow had reached steady value and does not change very much. To implement such a grid, a geometric series stretching was performed on the domain

. Figure 5 shows one such stretched grid with stretching ratio of 1.1 for a grid size NXN where, N=61.

IV. Results

During the computation, the norm of the difference between the old and new values of x-velocity was monitored. The solution was assumed to have converged when this norm had reached value lower than 10^{-6}. The computation was started with an initial velocity profile which is presented in fig. 6. First a grid independence study was carried out for Re_h=50 (*i.e* Re_D=*100*)for grid size ranging from 21×21 to 201×201. The change in norm values found in this study is represented in fig. 7. From this figure we can see that the change in norm values do not increase with any further increase in number of grid points at N=121. Hence we can conclude that the solution has become grid independent at N=121 for the considered domain (*i.e.*2h×20h, where h is the step size). Therefore, hereafter, all the computations have been carried out on a 121×121 grid.

Figures 8 and 9 show comparison between the fully developed velocity profile of Armaly *et al.*'s result and the result obtained during present study,respectively, for Re_D=100.

Figures 10-13 show streamlines and velocity profiles for uniform grid for Re_h=50, 100, 200 and 400; and, figures 14-17 show the streamlines and velocity profiles for stretched grid for the same Reynolds numbers.

As we can see from the figures, the length of separation increases with increase in Reynolds number. Also, at higher Reynolds number, multiple separation zones start forming. In literature, multiple flow separation zones have been reported at $Re_D > 500$. In our study, we observe this phenomenon for $Re_h = 400$(*i.e.* $Re_D = 800$). All other Reynolds number considered here are lower than 500, hence, we get only one recirculation region which is located under the step.

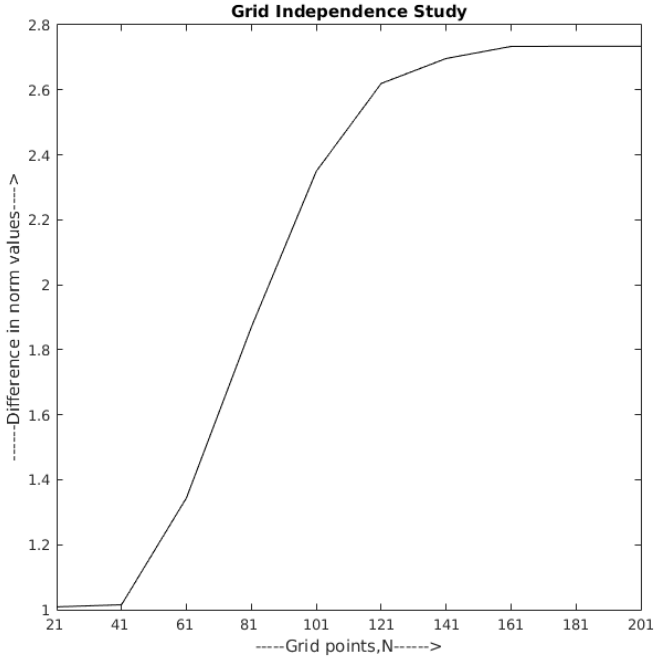

Figure 6: *Grid Independence study for Re_D=100*

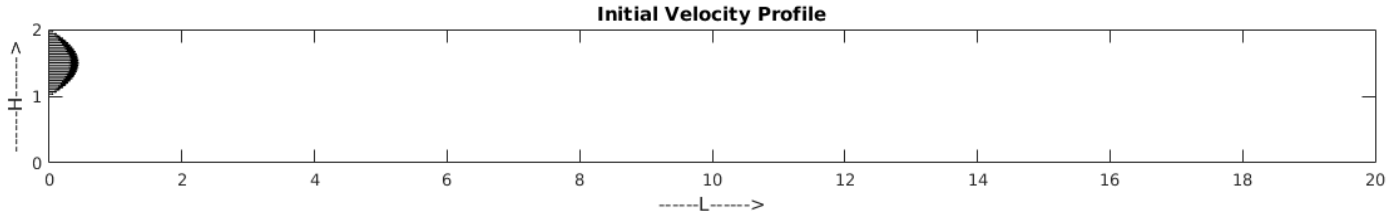

Figure 7: *Velocity profile of the inlet velocity*

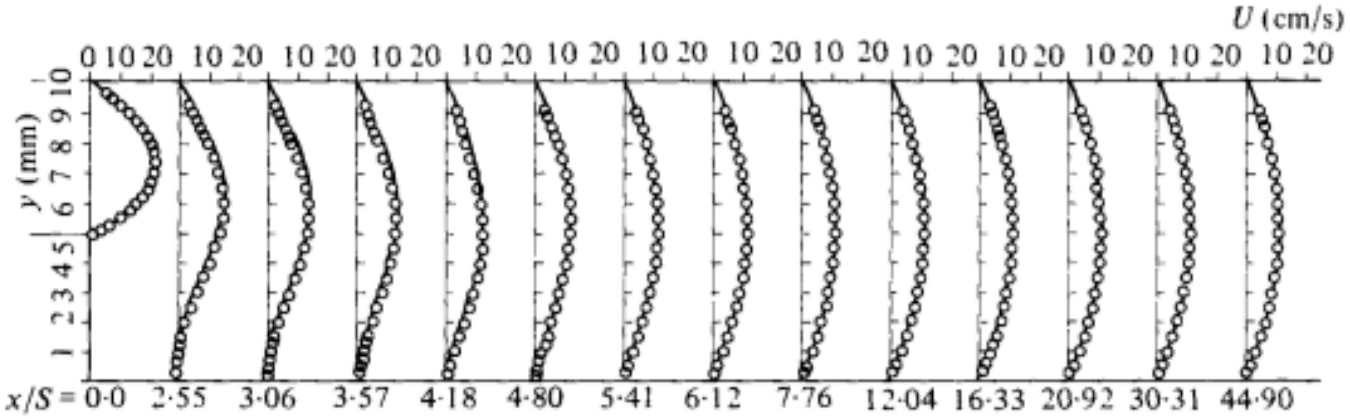

Figure 8: *Experimental velocity profile obtained by Armaly et al. for Re_D=100*

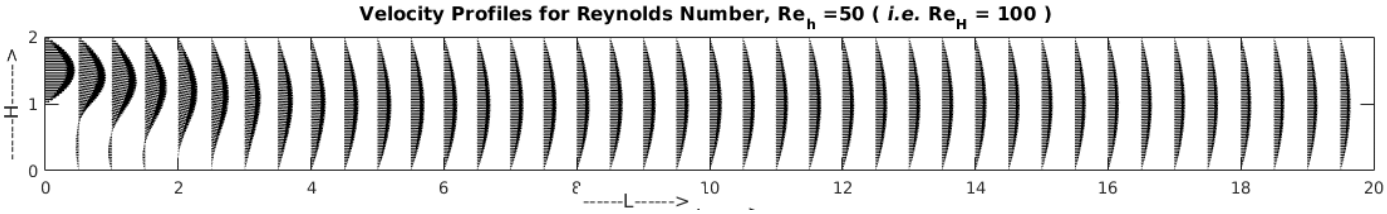

Figure 9: *Velocity profile for Re_D =100*

I. Uniform Grid

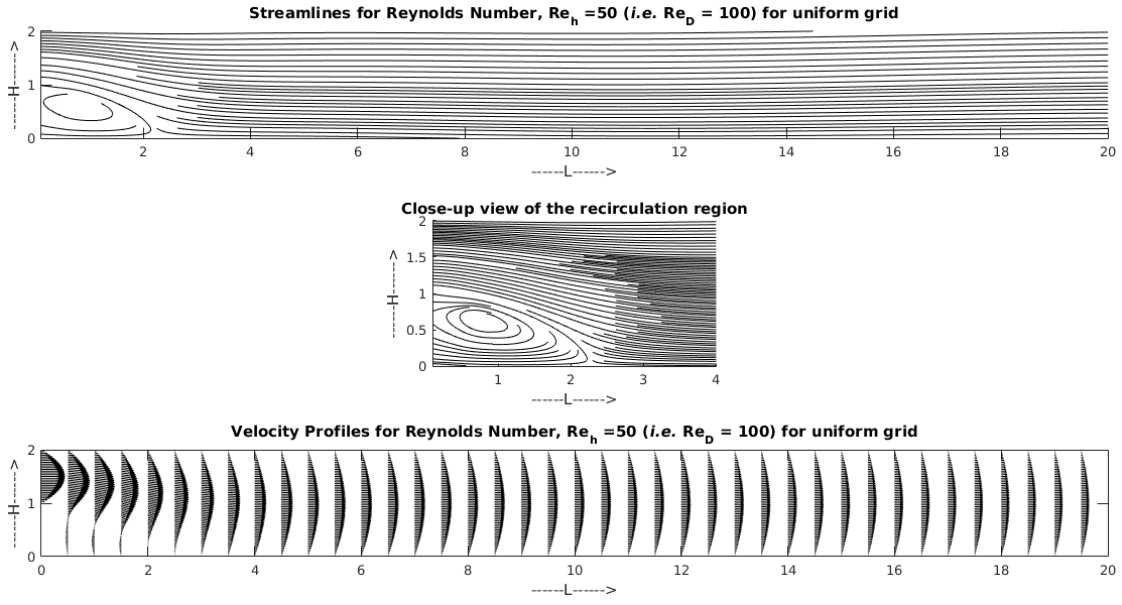

Figure 10: *Streamlines and Velocity profile for Re_h =50 for a uniform grid*

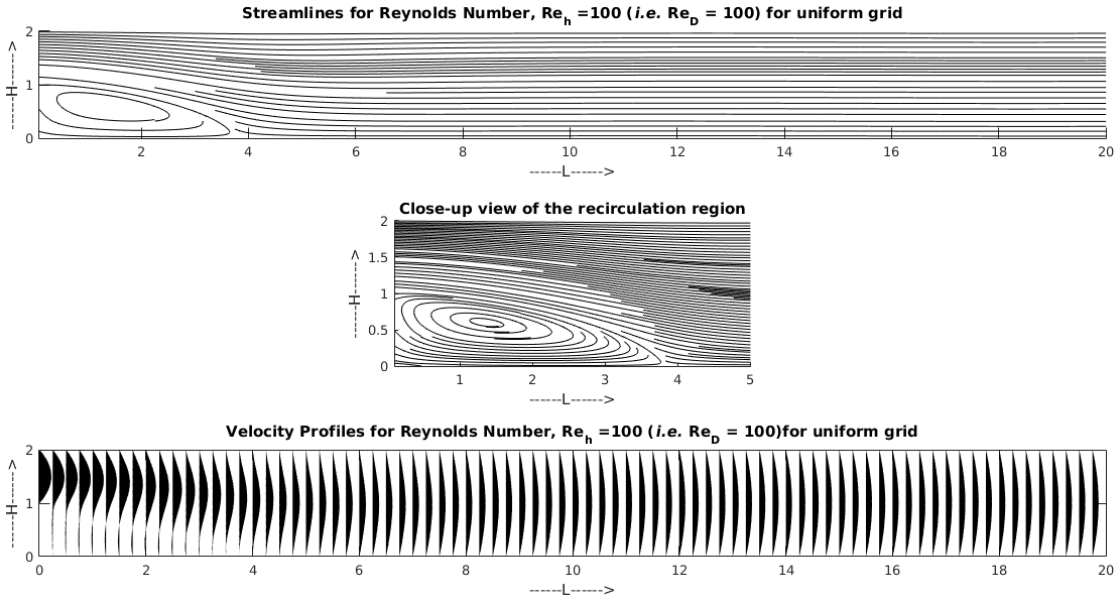

Figure 11: *Streamlines and Velocity profile for Re_h =100 for a uniform grid*

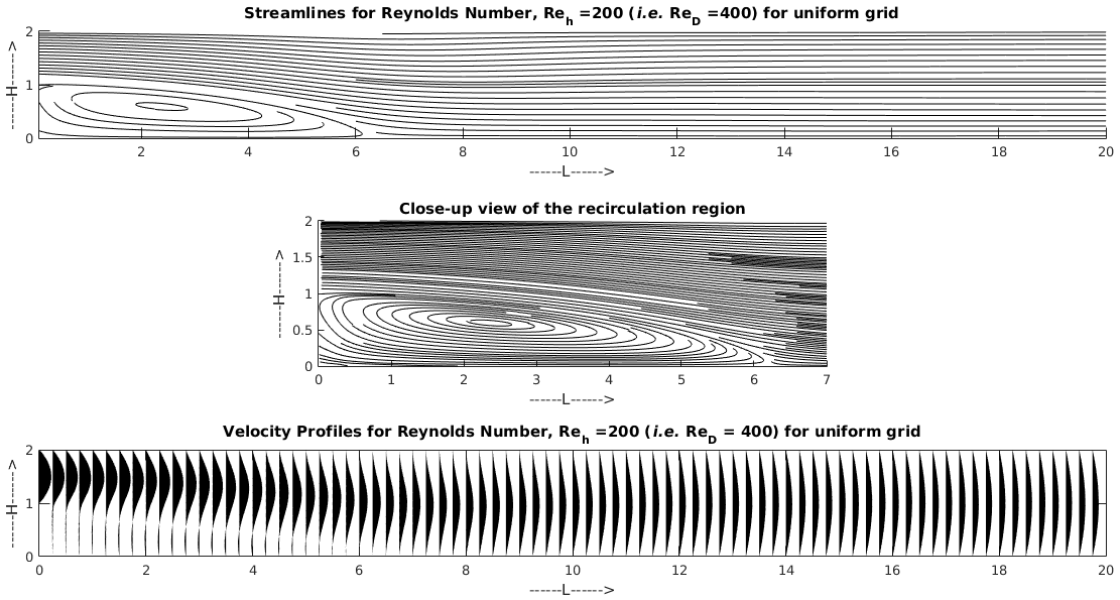

Figure 12: *Streamlines and Velocity profile for Re_h =200 for a uniform grid*

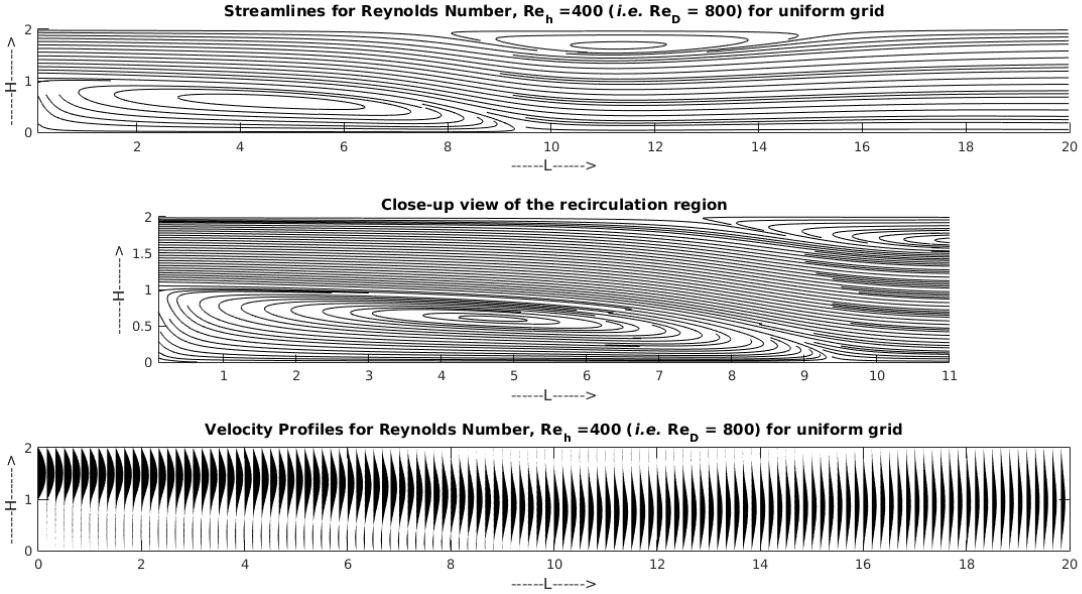

Figure 13: *Streamlines and Velocity profile for Re_h =400 for a uniform grid*

II. Stretched Grid

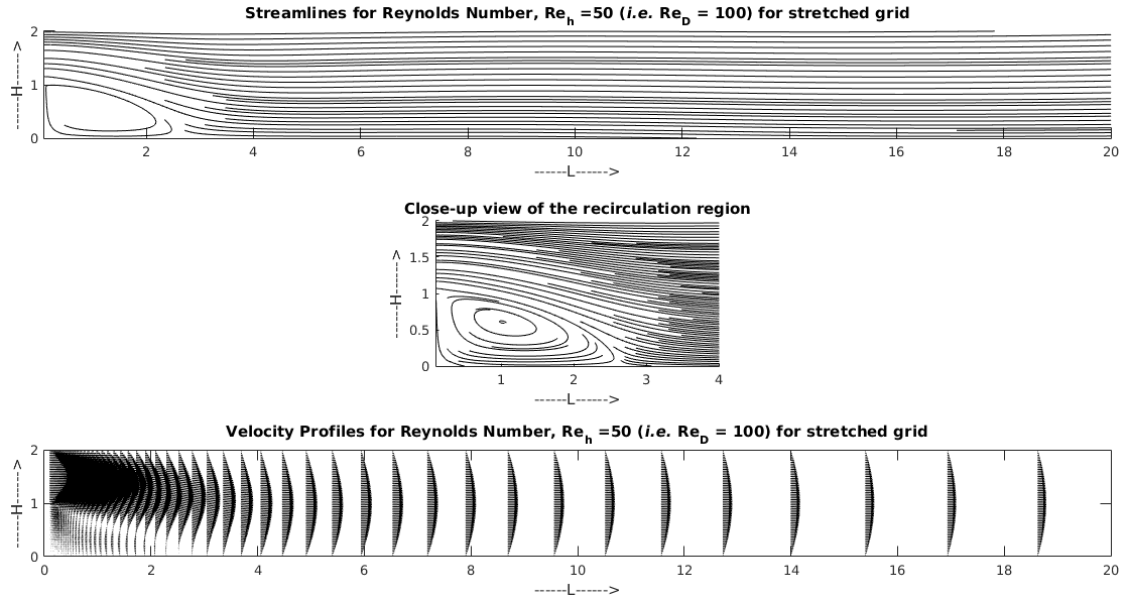

Figure 14: *Streamlines and Velocity profile for Re_h =50 for a stretched grid*

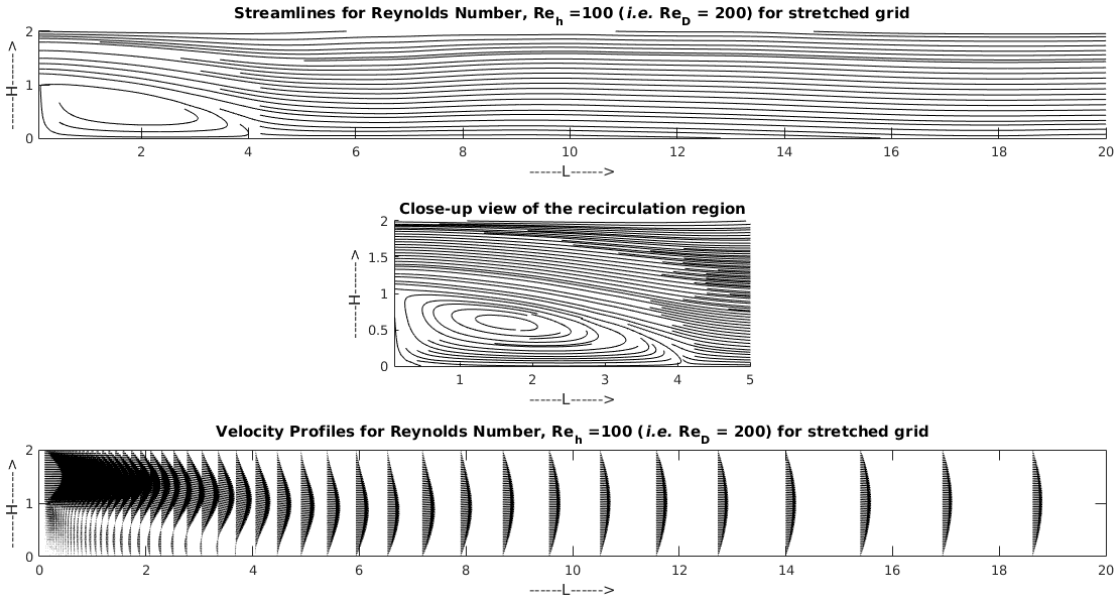

Figure 15: *Streamlines and Velocity profile for Re_h =100 for a stretched grid*

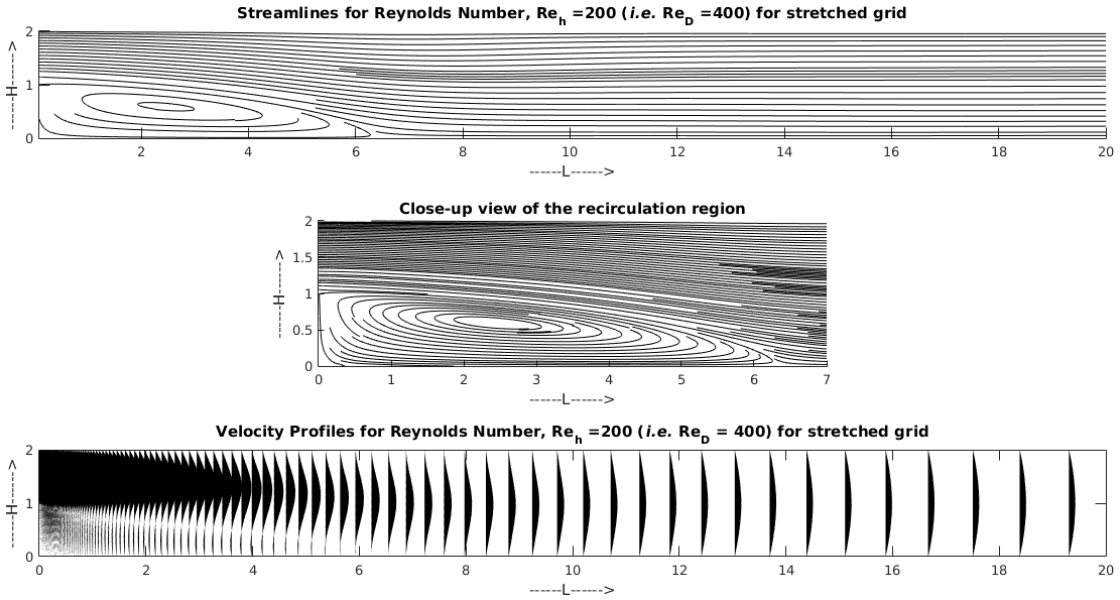

Figure 16: *Streamlines and Velocity profile for Re_h =200 for a stretched grid*

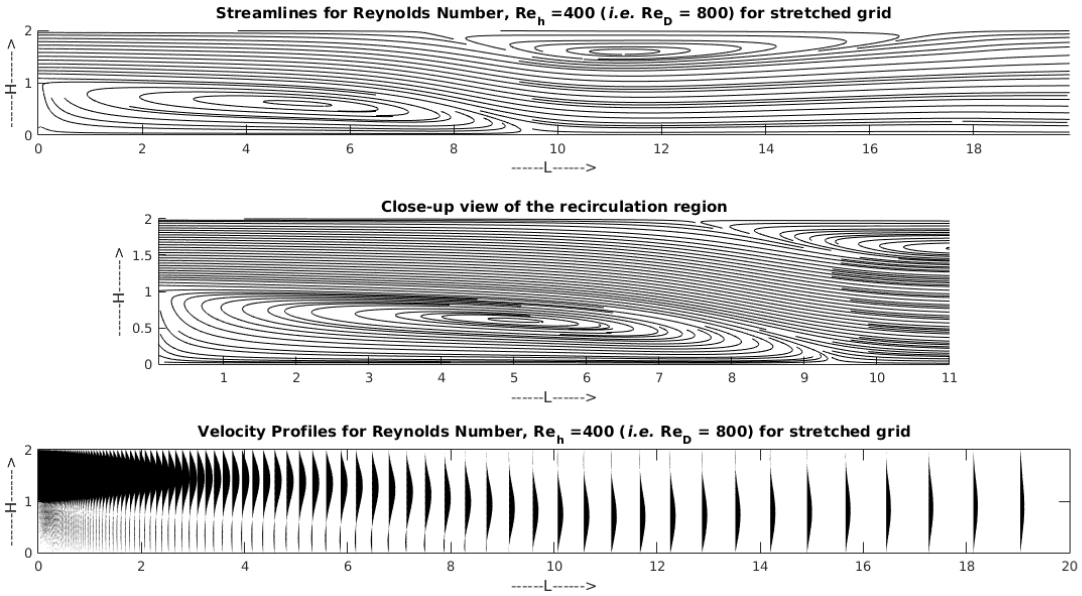

Figure 17: *Streamlines and Velocity profile for Re_h =400 for a stretched grid*

III. Comparison of computed results

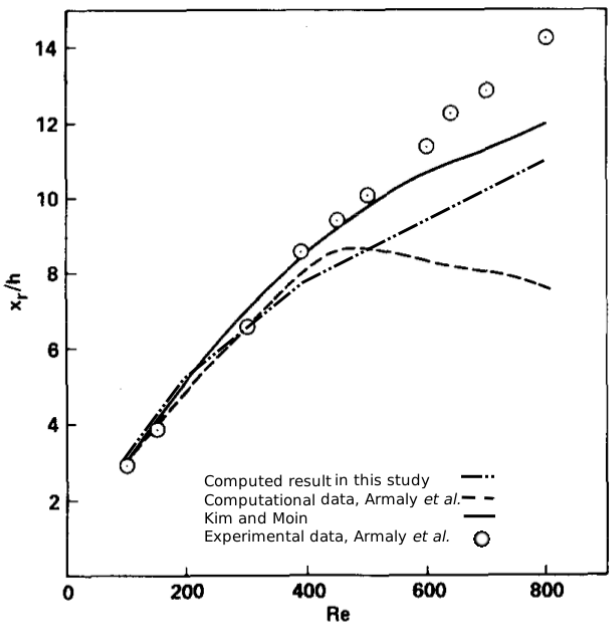

Figure 18: *Reattachment length as a function of Reynolds number*

In fig. 18, reattachment length is presented as a function of Reynolds number. The results are compared with computed results obtained by Armaly *et al.* and Kim and Moin. The experimental data presented by Armaly *et al.* are also presented to better understand difference in computational and experimental results. The computed results obtained show a larger reattachment length compared to those obtained by Armaly *et al.* but shorter than results obtained by Kim and moin. We can also observe that the computed results start to deviate from experimental results for Re_D >400, as reported in numerous works. This difference is not attributed to the numerical error in the solution but due to the three dimensionality of the flow which is due the formation of multiple flow separation zones for Re_D >400 as Armaly *et al.* have pointed out.

IV. Effect of local time stepping, implicit residual smoothing and the CFL number

Local time stepping helped in optimizing time stepping for each node since at some nodes, the CFL number might be different due to the fact that solution might not change at those nodes alot. This helped in reducing the number of iterations by a significant amount. Local time stepping was controlled by CFL and Von Neumann number. The CFL number was a very important factor in the calculations since the pseudo time step, $\Delta\tau$, depended on CFL number. A general observation during the calculations was that as Reynolds number increased, the CFL number had to be reduced in order to achieve a stable solution. For Re_h=50 it was found that the solution was

stable for CFL≤1, for Re_h=100 : CFL≤0.5, for Re_h=200 : CFL≤0.1, for Re_h=400 : CFL≤0.1. Implicit residual smoothing helped in reducing residuals and thus helps in achieving convergence faster in pseudo time. The effect of this phenomenon was oberved by running the calculations with and without residual soothing for Re_h=400. With a CFL of 0.1 and Von Nuemann number of 0.1, the solution took 4.2×10^5 iterations to converge without residual smoothing and with residual smoothing, it took 5.6×10^4 iterations to converge. Hence, we can conclude that residual smoothing had a great impact on the rate of convergence of the solution.

V. Effect of artificial dissipation on the accuracy and stability of the solution

Artificial dissipation reduces the ossicilations in the solution which increases accuracy and helped the solution achieve a more stable solution which was less prone to ossilations. Aritificial dissipation however also impacts the accuracy of the solution. In our calculations, we have taken dissipation factor of 0.01. On changing the disipation factor to 0.1, the reattachment length was effected by 20.3% for Re_h=400.

V. Summary

A 2D Navier-Stokes solver was developed to simulate steady, laminar flow over a backward-facing step of height h. The step expansion ratio=1/2 and the flow at the step was assumed to be fully developed, laminar channel flow. The 2D incompressible Navier-Stokes equations was solved in generalized curvilinear coordinates using artificial compressibility method. A code was developed using MATLAB where three-point , second order finite differencing was used to discretize the convective and viscous fluxes in conjunction with scalar, fourth-difference, third-order artificial dissipation for stability. Dual time-stepping with a second-order backward scheme in real time and four stage Runge-Kutta time stepping was used for pseudo time. A grid independence study was carried out and it was found that the soluton became grid independent at N=121. The flow was then simulated for Re_h=50, 100, 200, and 400. The streamlines and velocity profiles were plotted in the steady-state. The results were compared by comparing reattachment length presented the experimental data obtained by Armaly *et al.* and the numerical solutions obtained by Kim and Moin.

VI. Conclusion

The solution was in good agreement with results obtained by Armaly *et al.* and Kim and Moin. The reattachment length was found to be larger than Armaly *et al.* and shorter than Kim and Moin's result for $Re_D > 400$. It is also worth noting that using local time stepping and residual smoothing increased convergance rate of the solution by a significant amount. Also, using artificial dissipation helps in reducing ossilations and provides more stable results. However, too much dissipation in favour of a more stable solution could lead to incorrect reatteachment lengths.

References

[1] John David Anderson and J Wendt. *Computational fluid dynamics*, volume 206. Springer, 1995.

[2] Bassem F Armaly, F Durst, JCF Pereira, and B Schönung. Experimental and theoretical investigation of backward-facing step flow. *Journal of Fluid Mechanics*, 127:473–496, 1983.

[3] G Biswas, M Breuer, and F Durst. Backward-facing step flows for various expansion ratios at low and moderate reynolds numbers. *Journal of fluids engineering*, 126(3):362–374, 2004.

[4] Elba Bravo, Julio R Claeyssen, and Rodrigo B Platte. A direct one-step pressure actualization for incompressible flow with pressure neumann condition. *Journal of computational and applied mathematics*, 103(1):43–53, 1999.

[5] TP Chiang, Tony WH Sheu, and CC Fang. Numerical investigation of vortical evolution in a backward-facing step expansion flow. *Applied Mathematical Modelling*, 23(12):915–932, 1999.

[6] Alexandre Joel Chorin. A numerical method for solving incompressible viscous flow problems. *Journal of computational physics*, 2(1):12–26, 1967.

[7] Alexandre Joel Chorin. Numerical solution of the navier-stokes equations. *Mathematics of computation*, 22(104):745–762, 1968.

[8] Ercan Erturk. Numerical solutions of 2-d steady incompressible flow over a backward-facing step, part i: High reynolds number solutions. *Computers & Fluids*, 37(6):633–655, 2008.

[9] Boyce E Griffith. An accurate and efficient method for the incompressible navier–stokes equations using the projection method as a preconditioner. *Journal of Computational Physics*, 228(20):7565–7595, 2009.

[10] Klaus A Hoffmann and Steve T Chiang. {*Computational fluid dynamics, Vol. 1*}. 2000.

[11] John Kim and Parviz Moin. Application of a fractional-step method to incompressible navier-stokes equations. *Journal of computational physics*, 59(2):308–323, 1985.

[12] Hans Petter Langtangen, Kent-Andre Mardal, and Ragnar Winther. Numerical methods for incompressible viscous flow. *Advances in Water Resources*, 25(8):1125–1146, 2002.

[13] JC Mandal and Anesh S Iyer. An upwind method for incompressible flow computations using pseudo-compressibility approach. In *19th Computational Fluid Dynamics Conference*, pages 22–25, 2009.

[14] Socrates Vrahliotis, Theodora Pappou, and Sokrates Tsangaris. Artificial compressibility 3-d navier-stokes solver for unsteady incompressible flows with hybrid grids. *Engineering Applications of Computational Fluid Mechanics*, 6(2):248–270, 2012.